Sensors and Actuators A 253 (2017) 27–34

Contents lists available at ScienceDirect

Sensors and Actuators A: Physical

journal homepage: www.elsevier.com/locate/sna

Microblower-based microfluidic pump

Xinran Wang, Huawei Jiang, Yuncong Chen, Xuan Qiao, Liang Dong*

Department of Electrical and Computer Engineering, Iowa State University, Ames, IA, 50011, USA

ARTICLE INFO

Article history:
Received 9 June 2016
Received in revised form 9 November 2016
Accepted 12 November 2016
Available online 15 November 2016

Keywords:
Microblower
Miniaturized pump
MEMS
Fluid manipulation

ABSTRACT

This paper reports on a highly economical and accessible microfluidic pump using a piezoelectric air microblower for the controlled pumping of small-volume fluids into microfluidic chips. The present pump exerts high-accuracy control over the driving pressure to deliver fluids into and flexibly alter their flow rate inside microfluidic channels with a fast response at the millisecond scale and high pumping pressure stability. We have demonstrated the applications of this pump to shift the fluidic interface between laminar flows across a microfluidic channel, produce microdroplets with controllable sizes and chemical ingredients, and generate a discrete concentration gradient when incorporating a microfluidic concentration generator. Owing to its easy assembly and low cost, the microfluidic pump can provide a highly accessible and inexpensive solution to pumping and manipulating liquids in microfluidic devices for many chemical and biological studies, and will be particularly suitable for applications requiring full system integration and flow rate control automation within a limited space and financial budget.

1. Introduction

Miniaturized microfluidic pumps have attracted much attention owing to the high demand to manipulate fluids at the microscale in many microfluidic lab-on-a-chip platforms. Numerous efforts have been made to develop micropumping technologies based on different mechanisms, such as electromagnetic actuation [1–3], piezoelectric vibration [4,5], thermo-pneumatic actuation [6,7], chemical reactions [8,9], capillary drag [10–12], and degas-driven flow [13,14]. Although commercial syringe pumps are widely used in research and clinical laboratories and offer high accuracy and robustness, their high cost impedes their extensive use in many portable microfluidic applications, especially when a number of pumps are needed to deliver different fluids at controlled flow rates. Another type of pump often used in microfluidic applications owing to its small size and low cost is the peristatic pump; however, its flexibility and accuracy of controlling the flow rate are relatively low. In addition, the delivery tubings of peristaltic pumps often need to be elastomeric to maintain a circular cross section after multiple cycles of squeezing and releasing. This requirement reduces the range of liquids that are compatible with these tubings, especially in chemical experiments [15].

The recent advances in micro-electro-mechanical systems (MEMS) technology have led to inexpensive commercial microblowers at a unit price of less than ten U.S. dollars (MZB1001T02; Murata Manufacturing, Kyoto Prefecture, Japan). The microblower has a compact footprint area of 20 mm by 20 mm and a thickness of 1.85 mm. Owing to its piezoelectric drive system, it consumes much lower power than common air-compressed devices. Basically, this microblower operates on the principle of the piezoelectric effect [16]. As shown in Fig. 1(b), the piezoelectric element is attached to a flexible diaphragm. When driven by a voltage, in a certain half period, the diaphragm vibrates at a predetermined frequency to draw air into the central cavity above the diaphragm; in the next half period, the air is discharged to provide an ejection flow rate that is greater than or equal to that corresponding to the displacement volume of the vibrating diaphragm. An increase in the applied voltage can lead to an increase in air pressure at the output nozzle of the microblower. Recently, this microblower has been used to develop a pneumatically tunable antenna capable of reconfiguring its radiation directivity [17].

In this paper, we report on a highly economical and accessible microfluidic pump that utilizes a miniature microblower to control the driving pressure for delivering fluids into and controlling their flow rate inside microfluidic devices with high flexibility, good accuracy and fast response. The simple design, low cost, and easy assembly render the proposed pump suitable for portable microfluidic applications.

* Corresponding author.
E-mail address: ldong@iastate.edu (L. Dong).

http://dx.doi.org/10.1016/j.sna.2016.11.017

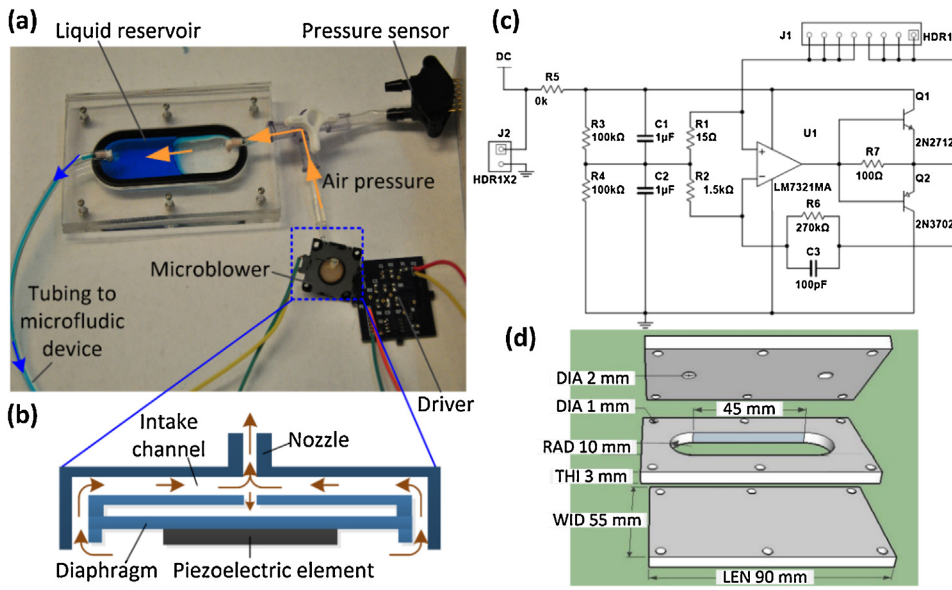

Fig. 1. (a) Microblower-based microfluidic pump. (b) Cross-sectional schematic of the microblower used in the proposed pump in (a). (c) Driver circuit of the microblower. (d) Schematic and dimensions of a typical horizontal liquid reservoir.

2. Structures, materials, and assembly

The microfluidic pump was composed of a microblower, an electronic driver, a horizontal liquid reservoir, and input and output tubings (Fig. 1(a)). The driver circuit converted the applied DC voltage (9–21 V) to an AC voltage for driving the microblower (Fig. 1(c)). Once the voltage was applied, a high-pressure air flow was generated, which exited from the outlet nozzle of the microblower and then flowed into a horizontally placed solution reservoir (Fig. 1(a) and (d)). To form the reservoir, a shallow cavity was machined through the entire thickness of a 3-mm-thick poly(methyl methacrylate) (PMMA) sheet (Acrylite Plexiglass; Midwest Plastics, Omaha, NE) using a milling machine (Mini-Mill/GX, MiniTech, Norcross, GA). The formed cavity was then sandwiched between two other PMMA sheets with an O-ring (oil-resistant Buna-N; McMaster-Carr, Elmhurst, IL) and six stainless-steel screw nuts (M1; Accuscrews, Huddersfield, UK). The typical dimensions of a 4.7 mL-volume reservoir are provided in Fig. 1(d). The solutions to be pumped were loaded into the reservoir through the corresponding inlet. Subsequently, the air outlet nozzle of the microblower was connected with the input tubing of the reservoir (inner diameter or ID = 1 mm, Tygon tubing; Cole-Parmer, Vernon Hills, IL) and the microfluidic pump was ready to use. The horizontal design of the reservoir can eliminate the effect of gravity on the flow rate of solutions injected into a microfluidic device. This is because when the pressurized fluids leave the reservoir, they can exit the outlet of the reservoir horizontally while keeping the surface level of the fluids consistently in contact with the top PMMA sheet. If a vertical reservoir was used, the surface level of the solutions would decrease as the liquids were pumped out, reducing the gravity-induced pressure on the connected microfluidic channels and thus causing variations in the flow rate of the solutions in the channels. In contrast, the horizontal design of our reservoir can provide a constant output flow rate for a given voltage applied to the microblower, without requiring a feedback electrical circuit to compensate for pressure variations induced by liquid level changes.

To demonstrate the applications of the pump, three polydimethylsiloxane (PDMS)-based microfluidic devices were fabricated. The first PDMS device was used to demonstrate the control of the fluidic interface between laminar flows and the other two to demonstrate the generation of microdroplets and the discrete concentration gradient of a chemical. These devices were manufactured using a conventional soft lithography technique [18]. Briefly, the patterns were designed with AutoCAD software (Autodesk, San Rafael, CA, USA) and a master mold made of SU-8 photoresist (SU-8-50, Microchem, Westborough, MA, USA) was then formed on a silicon wafer using conventional photolithography. A two-part curing PDMS precursor solution (A:B weight ratio = 10:1; Dow Corning, Midland, MI) was mixed and then degassed in a home-made chamber for 30 min under vacuum (10^{-4} Torr). The degassed PDMS solution was then poured over the master mold in a disposable polystyrene petri dish (diameter: 100 mm; Sigma-Aldrich, St. Louis, MO) and baked on a hot plate at 80 °C for 2 h. After thermal curing, the PDMS slab containing the channels was peeled off from the master mold. The inlet and outlet ports of the PDMS device were then manually punched with a mechanical puncher (diameter: 1 mm; Acuderm, Fort Lauderdale, FL). Lastly, the PDMS slab was bonded to a microscope glass slide (75 mm × 50 mm × 0.9 mm; Corning Inc., Corning, NY) through oxygen plasma treatment.

3. Results and discussion

3.1. *Driving pressure, flow rate, stability, and response time*

The stability of the driving air pressure is a critical factor for a high-performance microfluidic pump. Thus, an air-pressure sensor (SPD015AA; Smartec, The Netherlands) was used to monitor the pressure of the air exiting the output nozzle of the microblower. This air pressure was determined by the DC voltage applied to the driver circuit and was observed to linearly increase with the applied voltage (Fig. 2(a)). The air pressure stability was analyzed by testing the variance of the air pressure over a period of time under a certain driving voltage. As shown in Fig. 2(b), at the driving voltages 9, 12, 15, 18, and 21 V, the maximum pressure variation over 30 min was only 0.22 kPa or 0.7% of the full scale.

The driving voltage and the size of the tubing also affect the output flow rate of fluids from the liquid reservoir. In this experiment, microfluidic tubing (Tygon tubing; Cole-Parmer, Vernon Hills, IL) with the inner diameter of *ID* was connected to the output of the storage reservoir. A ruler was used to measure the moving distance of fluids d along the tubing at different time points t (shown in Fig. 3(a)). The average volumetric flow rate of flu-

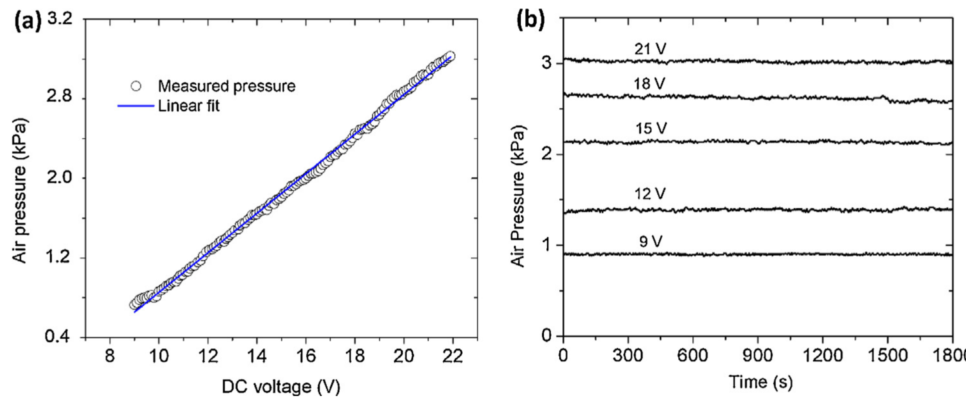

Fig. 2. (a) Air pressure at the output nozzle of the microblower as a function of applied driving voltage. (b) Air pressure at the output nozzle of the microblower over a 30-min period under different driving voltages.

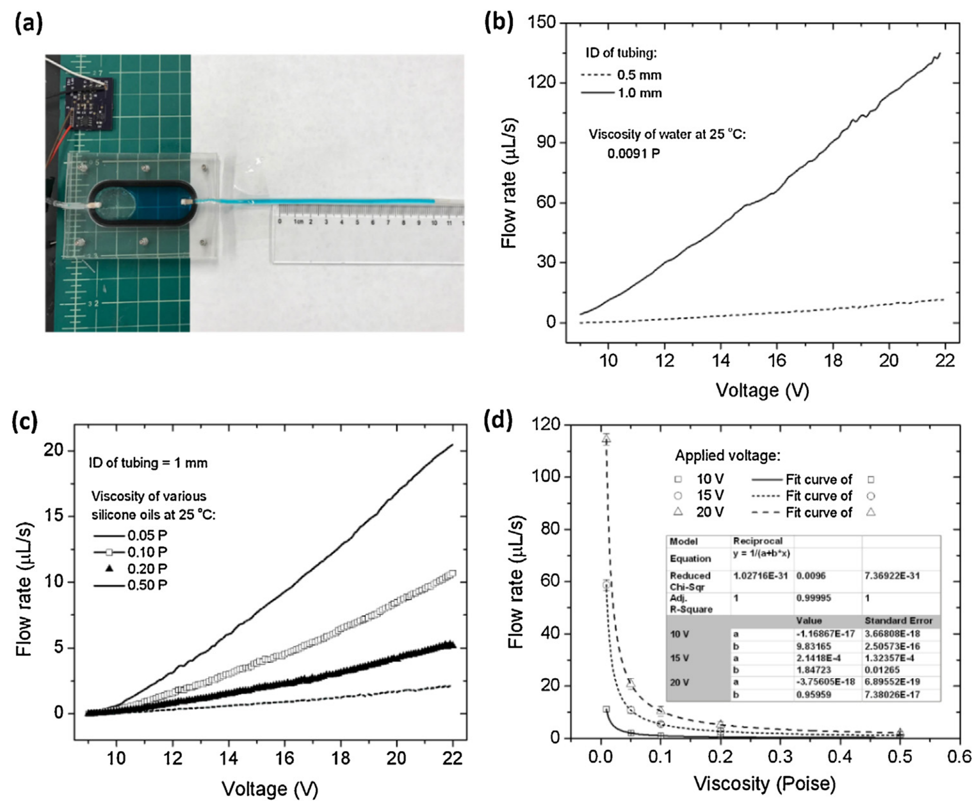

Model	Reciprocal		
Equation	y = 1/(a+b*x)		
Reduced Chi-Sqr	1.02716E-31	0.0096	7.36922E-31
Adj. R-Square	1	0.99995	1
		Value	Standard Error
10 V	a	-1.16867E-17	3.66808E-18
	b	9.83165	2.50573E-16
15 V	a	2.1418E-4	1.32357E-4
	b	1.84723	0.01265
20 V	a	-3.75605E-18	6.89552E-19
	b	0.95959	7.38026E-17

Fig. 3. (a) Experimental setup for flow rate measurement. (b) Flow rates of water flowing in 0.5 mm- and 1.0 mm-ID tubings as a function of applied voltage. (c) Flow rate of silicone oils with different viscosities flowing in a 1.0 mm-ID tubing as a function of applied voltage. (d) Flow rate of water and silicone oils with different viscosities flowing in a 1.0 mm-ID tubing at applied voltages of 10, 15, and 20 V. The inset table shows the fitting parameters of a reciprocal function for flow rate with respect to fluid viscosity.

ids v pumped within a time period of Δt was calculated using $v = \pi \times (ID/2)^2 \times d/\Delta t$. Fig. 3(b) shows the relationship between the flow rate of water and the applied voltage for two different ID values of the connecting tubing. The results reveal that for a given tubing, the water flow rate linearly increased with increasing voltage from 8 to 22 V. The increase of the voltage led to an enhanced air pressure at the output nozzle of the microblower, thus increasing the water flow rate along the tubing. In addition, for a given voltage, the flow rate increased with increasing ID of the output tubing. According to Poiseuille's law [19], the fluidic resistance of laminar flow is given by Eq. (1):

$$R = \frac{8\eta L}{\pi r^4} \quad (1)$$

where η is the viscosity in dyn s/cm^2 (poise, P) (η = 0.0091 P for water at 25 °C) and r is the inner radius and L the length of the output tubing. Therefore, the fluidic resistance decreases with increasing tubing radius, thus increasing the flow rate. Fig. 3(c) shows the flow rate of silicone oils with different viscosities (0.05, 0.1, 0.2, and 0.5 P at 25 °C, all from Sigma-Aldrich, St. Louis, MO) flowing along a 1.0-mm-ID tubing at different applied voltages. Similar to the case of driving water, the flow rate of driving silicon oil increased linearly with increasing voltage; the higher the viscosity, the lower the flow rate. Fig. 3(d) summarizes the flow rates of water and silicone oils at applied voltages of 10, 15, and 20 V. The result demonstrates that the flow rate was proportional to the reciprocal of the viscosity.

To study how fast the driving pressure of the pump could respond to an applied voltage, we monitored the air pressure at

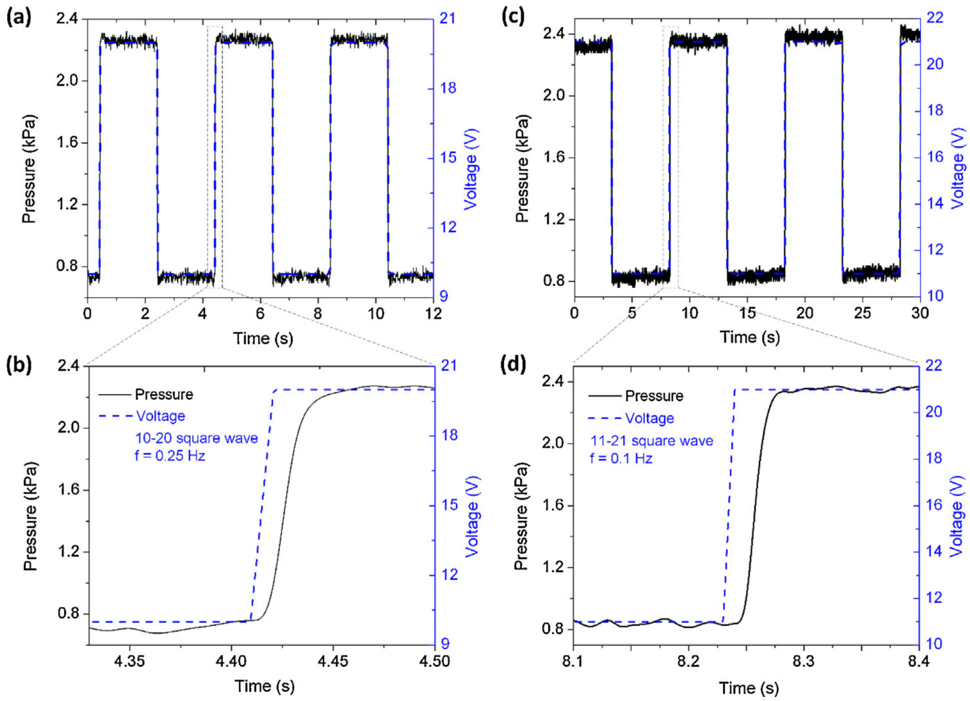

Fig. 4. Pressure at the output nozzle of the microblower under two different square-wave driving voltages: (a), (b) frequency f = 250 mHz, low potential V_L = 10 V, and high potential V_H = 20 V; (c), (d) f = 100 mHz, V_L = 10 V, and V_H = 20 V. (c) and (d) are the magnifications of (a) and (b) at time t = 4.35–4.50 s and t = 8.1–8.4 s, respectively.

the inlet of the liquid reservoir when a periodic square-wave voltage was applied to the driver circuit. The testing setup used in this experiment was the same as that shown in Fig. 1(a). Fig. 4(a) shows that the waveform of the output air pressure had almost the same shape as that of the applied voltage at a frequency of 0.25 Hz. The magnification of the rising edge of the input voltage and output air pressure in Fig. 4(b) indicates that the delay time from the input voltage onset to the stable output air pressure was approximately 40 ms. A similar response was observed when the frequency of the square-wave voltage changed to 0.1 Hz, as shown in Fig. 4(c) and (d).

Table 1 compares the characteristics between the microblower-based pump and other microfluidic pumps. It shows that the present pump exhibits considerable high accuracy and wide dynamic range of flow rate. The assembling of the pump is fairly simple, only involving minor needs of fabrication, which, in conjunction with the low cost of microblower (<$10 per unit), makes it highly accessible and useful for microfluidic applications requiring accurate and wide-range control of flow rate for conducting many experiments in parallel.

3.2. Control of fluidic interface between laminar flows

We demonstrated the control of the fluidic interface between laminar flows in a microfluidic channel using two microblower-based pumps A and B. The experimental setup is shown in Fig. 5(a). Pumps A and B were used to drive yellow and blue water solutions, respectively, into the channels (width: 70 μm; depth: 50 μm). A 20 V DC voltage was applied to pump A to control the flow rate of blue water and a triangular-wave voltage with a frequency of 0.2 Hz and amplitude varying between 16 V and 20 V was applied to pump B to inject yellow water into the device. 1.0 mm-ID tubings were used to realize fluidic connections between different components.

Fig. 5(b) displays time-lapse images showing the shifting of the interface between the two colored-water flows. During the first half period, the driving voltage of pump A was initially higher than that of pump B, causing the blue flow to move faster than the yellow one. This, in turn, resulted in the interface moving towards the yellow flow. As the flow rate of the yellow water gradually increased owing to the increase of the voltage applied to pump B, the interface of moved towards the blue flow until the applied voltage to pump B reached its highest value, 20 V. During the second half period, the interface shifted back towards the blue flow because the applied voltage decreases. Fig. 5(c) quantitatively describes the shift pattern of the interface with the triangular wave-voltage applied to pump B. The relative standard deviation of the interface position for six repeated measurements was as low as 6%, indicating the reliability of the pump.

3.3. Generation of microdroplets with controlled size and concentration

We demonstrated the implementation of two microblower-based pumps to generate microdroplets in a microfluidic device. In this demonstration, one horizontal reservoir was filled with orange water and the other one with silicone oil (viscosity = 5 P; Sigma-Aldrich, St. Louis, MO). Surfactant (Span 80, 2 wt%, Sigma-Aldrich, St. Louis, MO) was pre-added to the silicone oil to prevent droplet coalescence. Each reservoir was connected to a microblower. As shown in Fig. 6(a), water was pumped from the water reservoir into a horizontal channel (width: 100 μm; depth: 50 μm) through a 1 mm-ID tubing and oil was pumped from the oil reservoir into a vertical channel (width: 100 μm; depth: 50 μm) through the other 1 mm-ID tubing. The water flow was then pinched off by the oil flow at the T-shaped junction to form fine droplets. Fig. 6(a) shows that water droplets were formed when V_{water} = 18 V and V_{oil} = 22 V were applied to the water pump and the silicone oil pump, respectively. The diameter of these round droplets was 89.3 ± 5.2 μm (mean ± standard deviation, obtained from measurements for 50 droplets). As V_{water} increased from 10 to 20 V, while maintaining V_{oil} = 22 V, the diameter of the droplets increased, as demonstrated in Fig. 6(b). Fig. 6(c) shows that the larger plug-like droplets were generated when V_{water} = 16 V and V_{oil} = 14 V were applied to the two pumps. The resulting droplets, shown in Fig. 6(c), had length

Table 1
Comparisons of characteristics for different types of pumps used in microfluidic applications.

Pumping method	Flow rate (mL/min)	Flow pattern	Size (mm^3)	Accuracy	Features
Commercial syringe pump[a]	1e−10 to 128	Continuous or pulsatile	18 0× 27 0× 210	± < 0.04%	Commercial product; stable; high accuracy
Electroactive polymer [20,21]	Up to 0.025 [20] Up to 0.0025 [21]	Continuous	2.2 × 2.2 × 0.08 [20] 30 × 12 × 5 [21]	11.7–16% [21]	Easy control; light weight; small size; low cost
Peristaltic pump [22]	Up to 2.74e + 5	Pulsatile	168.3 × 120.7 × 114.3	32.9%	Simple structure; low cost; easy control
Osmosis [23]	3.3e−4	Continuous or pulsatile	15 ×15 × 16	4.3%	Long-lasting constant flow; simple structure
Capillary force [24]	3.3e−9 to 6.1e−8	Continuous	10 × 0.03 × 0.03	<10%	Easy to operate; low cost
Gravity [25,26]	2.1e−5 [25] Up to 1.8 [26]	Continuous	20 ×0. 14 × 1 [25] 0.15 ×0. 067 × 0.055 [26]	NA	Good for low flow rates
Finger powered [27]	Up to 60	Pulsatile	10 × 10 × 2.5	<4.7%	Easy to operate and integrate with on-chip functions
Microblower (this work)	1e−10 to 128	Continuous or pulsatile	20 ×20× 1.85	± < 1%	High accuracy; low cost; easy to control

[a] Model #10060, Nexus 6000 High Pressure Syringe Pump.

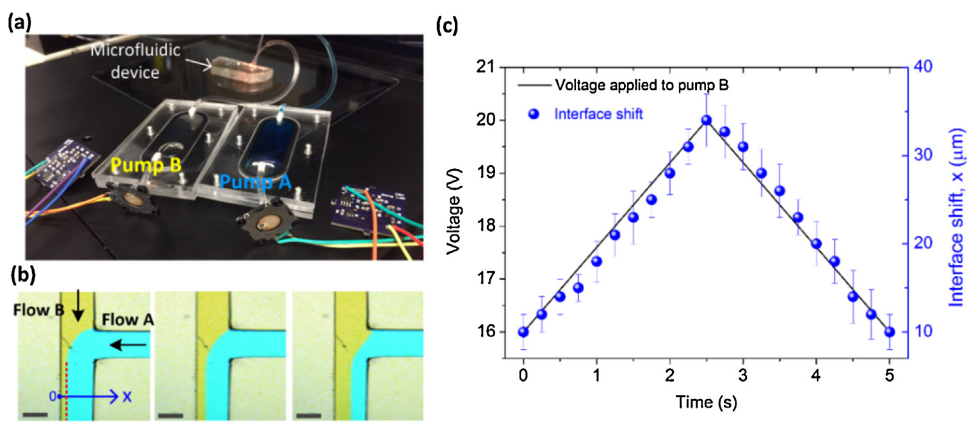

Fig. 5. (a) Setup for controlling the shift of the interface of laminar flows within a microfluidic device using two microblower-based pumps. (b) Time-lapse images showing that the interface between the blue flow B and yellow flow A shifts across the channel. The interface is indicated by a dashed red line in the first panel of (b). The scale bars represent 50 μm. (c) Quantitative shift of the interface as a function of voltage applied to pump B, which was used to control the yellow flow B. The black curve shows the applied triangular wave with a frequency of 0.2 Hz. The blue circles show the resulting shift of the interface at different time points within a cycle. (For interpretation of the references to colour in this figure legend, the reader is referred to the web version of this article.)

650.4 ± 40.6 μm. Similarly, the length of the droplets increased by increasing V_{water} from 12 to 18 V and fixing V_{oil} at 14 V, as shown in Fig. 6(d). The results demonstrate that the proposed pumps can generate droplets with well-controlled sizes in microfluidic devices.

Furthermore, we combined the capacity of the pump to control the fluidic interface between laminar flows and to generate droplets to demonstrate the formation of droplets with different chemical concentrations. As shown in Fig. 7(a), three pumps were used in this experiment, one for distributing blue water, one for clear water, and one for silicone oil (viscosity = 5 P). As expected, as the voltage applied to the blue-water pump decreased from 17 V to 14 V and then to 10 V and the voltage applied to the clear-water pump increased from 11 V to 15 V and then to 20 V, the interface between the two flows shifted towards the blue flow. These two water flows were then broken into droplets by the oil flow, which was driven by the oil flow pump, operating at a constant voltage of 16 V. Therefore, the droplets formed in every voltage condition had a different volume ratio between blue and clear water, as indicated by the color of the formed droplets. The relative standard deviation of the droplet size in the voltage conditions of Figs. 7(b)–(d) was ±6.9%, ±6.6%, and ±7.4%, respectively.

3.4. Generation of discrete concentration gradient

Fig. 8 demonstrates that the microblower-based pump can be combined with a microfluidic concentration gradient generator (CGG) to form concentration gradients of two chemicals. The CGG had two inlets and eight outlets. The serpentine channels of the CGG was 500-μm-wide and 100-μm-deep. Two pumps were used to continuously drive and infuse blue and yellow water from the corresponding reservoirs to the CGG through the two inlets (Fig. 8(a)). We observed that as the two input colored streams traveled through the CGG, they were repeatedly split at the nodes, combined with neighboring streams in a laminar fashion, and mixed by diffusion in the serpentine channels. At the outlets of the device, a discrete color gradient comprising eight colors created from blue and yellow were generated (Fig. 8(b)).

4. Conclusions

We demonstrated an inexpensive and easily fabricated miniature pump consisting mainly of a MEMS microblower and a horizontal solution reservoir. The flow rate of this pump can be continuously adjusted with good accuracy and a fast response time by controlling the DC driving voltage. Owing to its low cost, the

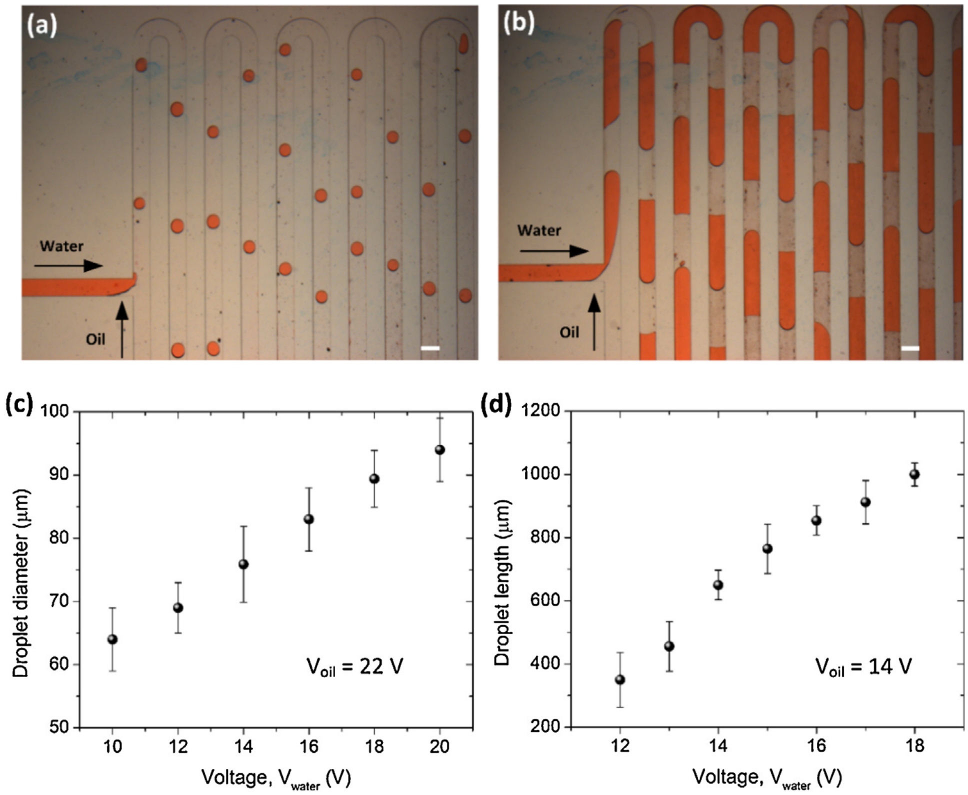

Fig. 6. (a), (b) Photographs showing the droplets generated by using two microblower-based pumps to control the flow rates of water and oil injections into the channels on a microfluidic droplet generator. In (a), V_{water} = 18 V and V_{oil} = 22 V. In (b), V_{water} = 16 V and V_{oil} = 15 V. The scale bars represent 100 µm. (c) Diameter of round droplets as a function of V_{water} at V_{oil} = 22 V. (d) Length of plug-like droplets as a function of V_{water} at V_{oil} = 14 V.

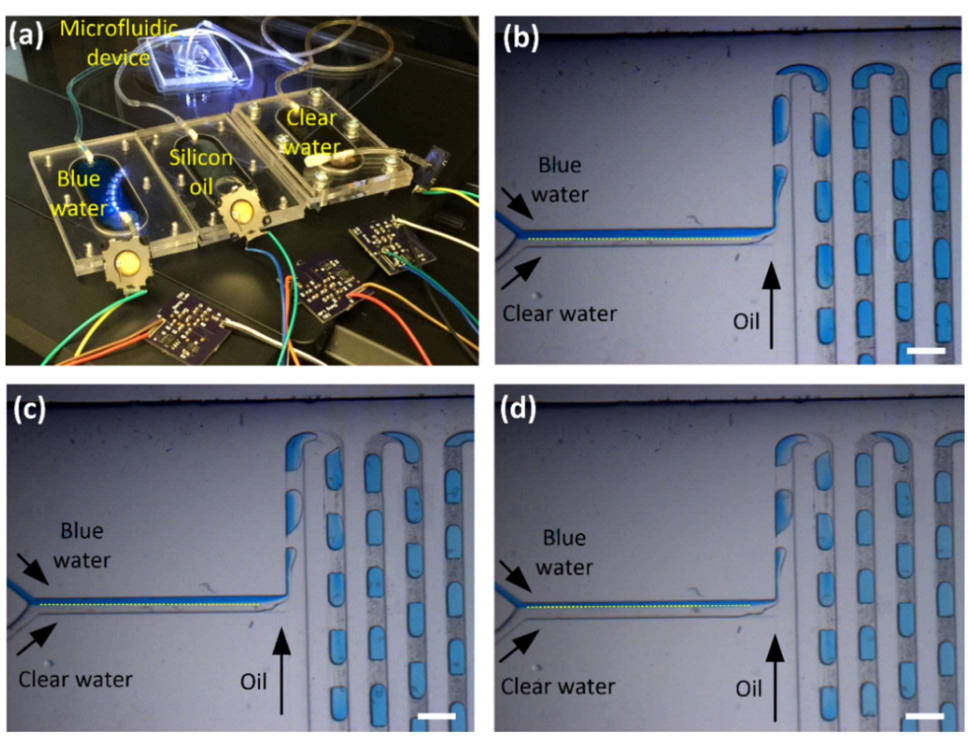

Fig. 7. (a) Setup for generating droplets with different chemical concentrations using three microblower-based pumps. (b)–(d) Droplets generated by a microfluidic device using the setup shown in (a). High (b), intermediate (c), and low (d) concentrations of blue dyes are mixed into the corresponding droplets by shifting and stabilizing the blue-clear water interface in the horizontal channel using the pumps. The scale bars represent 200 µm. (For interpretation of the references to colour in this figure legend, the reader is referred to the web version of this article.)

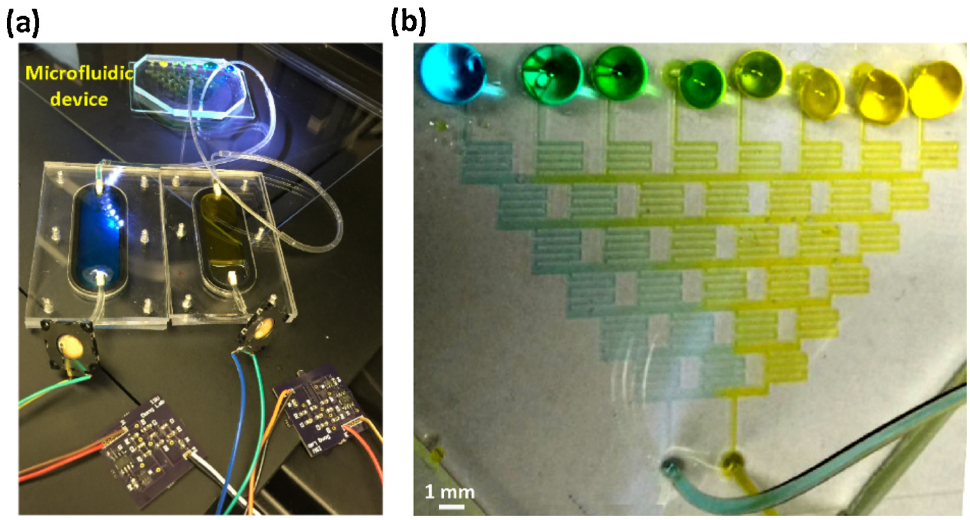

Fig. 8. (a) Setup for generating a concentration gradient using two microblower-based microfluidic pumps. (b) Eight different concentrations generated at the outputs of a microfluidic device using the setup shown in (a).

device is particularly suitable for applications requiring full system integration and flow rate control automation, especially when a number of miniature pumps need to be used within a limited space and financial budget.

Acknowledgements

This work was supported in part by the U.S. National Science Foundation under grants DBI-1353819, IOS-1650182, and ECCS-1102354, and the Iowa State University's Plant Sciences Institute.

References

[1] Q. Gong, Z. Zhou, Y. Yang, X. Wang, Design, optimization and simulation on microelectromagnetic pump, Sens. Actuators A-Phys. 83 (2000) 200–207.
[2] A. Hatch, A.E. Kamholz, G. Holman, P. Yager, K.F. Böhringer, A ferrofluidic magnetic micropump, J. Microelectromech. Syst. 10 (2001) 215–221.
[3] M. Shen, C. Yamahata, M.A. Gijs, Miniaturized PMMA ball-valve micropump with cylindrical electromagnetic actuator, Microelectron. Eng. 85 (2008) 1104–1107.
[4] J. Kan, Z. Yang, T. Peng, G. Cheng, B. Wu, Design and test of a high-performance piezoelectric micropump for drug delivery, Sens. Actuators A-Phys. 121 (2005) 156–161.
[5] O.C. Jeong, K. Satoshi, Fabrication of a peristaltic micro pump with novel cascaded actuators, J. Micromech. Microeng. 18 (2008) 025022.
[6] V.D.F. Pol, D.G.J. Wonnink, M. Elwenspoek, J.H.J. Fluitman, A thermo-pneumatic actuation principle for a microminiature pump and other micromechanical devices, Sens. Actuators A-Phys. 17 (1989) 139–143.
[7] W.H. Song, J. Lichtenberg, Thermo-pneumatic, single-stroke micropump, J. Micromech. Microeng. 15 (2005) 1425–1432.
[8] M. Koch, C.G. Schabmueller, A.G. Evans, A. Brunnschweiler, Micromachined chemical reaction system, Sens. Actuators A-Phys. 74 (1999) 207–210.
[9] D. Juncker, H. Schmid, U. Drechsler, H. Wolf, M. Wolf, B. Michel, N.D. Rooij, E. Delamarche, Autonomous microfluidic capillary system, Anal. Chem. 74 (2003) 6139–6144.
[10] J. Darabi, H. Wang, Development of an electrohydrodynamic injection micropump and its potential application in pumping fluids in cryogenic cooling systems, J. Microelectromech. Syst. 14 (2005) 747–755.
[11] Y.X. Guan, Z.R. Xu, Z.L. Fang, The use of a micropump based on capillary and evaporation effects in a microfluidic flow injection chemiluminescence system, Talanta 68 (2006) 1384–1389.
[12] L.W. Pan, Y.C. Su, S. Li, L. Lin, A disposable capillary micropump using frozen water as sacrificial layer, Proc. Hilton Head'02 (2002) 293–296.
[13] Y.H. Choi, S.U. Son, S.S. Lee, A micropump operating with chemically produced oxygen gas, Sens. Actuators A-Phys. 111 (2004) 8–13.
[14] L. Xu, H. Lee, D. Jetta, K.W. Oh, Vacuum-driven power-free microfluidics utilizing the gas solubility or permeability of polydimethylsiloxane (PDMS), Lab Chip 15 (2015) 3962–3979.
[15] M.A. Unger, H.P. Chou, T. Thorsen, A. Schereer, S.R. Quake, Monolithic microfabricated valves and pumps by multilayer soft lithography, Science 288 (2000) 113–116.
[16] K. Shungo, K. Gaku, K. Yoko, Piezoelectric microblower, US patent 8684707 B2. 2014, April 1.
[17] P. Liu, S. Yang, M. Yang, X. Wang, J. Song, L. Dong, Directivity-reconfigurable wideband two-arm spiral antenna, IEEE Antennas Wirel. Propag. Lett. (2016), http://dx.doi.org/10.1109/lawp.2016.2555941.
[18] H. Jiang, Z. Xu, M.R. Aluru, L. Dong, Plant-chip for high-throughput phenotyping of Arabidopsis, Lab Chip 14 (2014) 1281–1293.
[19] J. Pfitzner, Poiseuille and his law, Anaesthesia 31 (1976) 273–275.
[20] F. Xia, S. Tadigadapa, Q.M. Zhang, Electroactive polymer based microfluidic pump, Sens. Actuators A: Phys. 125 (2) (2006) 346–352.
[21] Y. Wu, D.Z. Zhou, G.M. Spinks, Pr. C. Innis, W.M. Megill, G.G. Wallace, TITAN: a conducting polymer based microfluidic pump, Smart Mater. Struct. 14 (2005) 1511.
[22] J. Xiang, Z. Cai, Y. Zhang, W. Wang, A micro-cam actuated linear peristaltic pump for microfluidic applications, Sens. Actuators A 251 (2016) 20–25.
[23] Z.R. Xu, C.G. Yang, C.H. Liu, Z. Zhou, J. Fang, J.H. Wang, An osmotic micro-pump integrated on a microfluidic chip for perfusion cell culture, Talanta 80 (3) (2010) 1088–1093.
[24] M. Zimmermann, H. Schmid, P. Hunziker, E. Delamarche, Capillary pumps for autonomous capillary systems, Lab Chip 7 (2007) 119–125.
[25] Glenn M. Walker, J.B. David, A passive pumping method for microfluidic devices, Lab Chip 2 (2002) 131–134.
[26] P. Morier, V. Christine, E.M. Philippe, R. Frédéric, S.R. Joël, Gravity-induced convective flow in microfluidic systems: electrochemical characterization and application to enzyme-linked immunosorbent assay tests, Electrophoresis 25 (2004) 3761–3768.
[27] K. Iwai, K.C. Shih, X. Lin, T.A. Brubaker, R.D. Sochol, L. Lin, Finger-powered microfluidic systems using multilayer soft lithography and injection molding processes, Lab Chip 14 (2014) 3790–3799.

Biographies

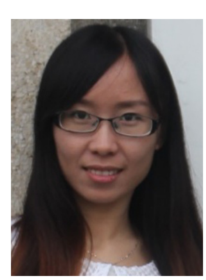

Xinran Wang received her B.S. degree in Electrical Engineering from Wuhan University, China in 2011 and M.S. degree from Wuhan Institute of Physics and Mathematics, China Academy of Sciences, in 2014. She is currently a doctoral student in Electrical Engineering at Iowa State University, Ames, Iowa, USA. Her research interests include sensors, electronics and biochips for sustainable agriculture.

Dr. Huawei Jiang received her Ph.D. degree in Electrical Engineering from the Department of Electrical and Computer Engineering at Iowa State University, Ames, Iowa, USA, in 2016. She also received her M.S. degree in Chemical Engineering from Dalian University of Technology, Dalian, China, in 2010. Currently, she is Post-Doctoral Research Associate in the Laboratory for MEMS and Biochips at Iowa State University. Her research is focused on development of microfluidic devices for plant phenotyping and microbial fuel cells.

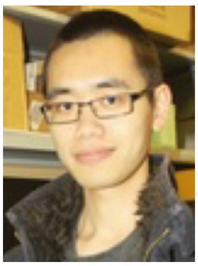

Yuncong Chen received his B.S. degree in Electrical Engineering from Iowa State University, Ames, Iowa, USA, in 2013. He is currently a graduate student in Electrical Engineering in the same institute. His research interest includes microfluidics, sensors and lab on a chip.

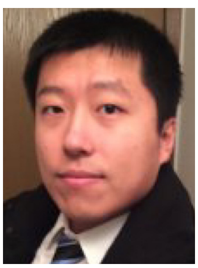

Xuan Qiao received his B.S. degree in Electrical Engineering from Iowa State University in 2014. He is currently a graduate student in Electrical Engineering in the same institute. His research interest includes microfluidics and lab on a chip for high-throughput assays and analysis.

Dr. Liang Dong is an Associate Professor in the Department of Electrical and Computer Engineering at Iowa State University (ISU). He is also affiliated with the Department of Chemical and Biological Engineering, the Microelectronics Research Center, and the Plant Sciences Institute at ISU, as well as the U.S. DOE's Ames Laboratory. He received his Ph.D. degree in Electronic Science and Technology from the Institute of Microelectronics at Tsinghua University, Beijing, China in 2004. From 2004 to 2007, he was a postdoctoral research associate in the Department of Electrical and Computer Engineering at University of Wisconsin-Madison. He serves as an Editorial Board membrane for the journal Science Reports and a guest editor for the journal Micromachines. He received the National Science Foundation CAREER Award, the Early Career Engineering Faculty Research Award, the Harpole-Pentair Developing Faculty Award, and the Warren B. Boast Undergraduate Teaching Award at Iowa State University. Before he came to the U.S., he received the Top 100 National Outstanding Doctoral Dissertation Award in China, and was one of the ten recipients of the Academic Rising Stars in Tsinghua University. His current research interests include MEMS, microfluidics, sensors, nanophotonics, and micro/nanomanufacturing and their applications in sustainable agriculture and environments, plant sciences, biomedicine, and internet of things.